BILL HOOD'S
SUPPLEMENTAL INFORMATION FOR STOPS 6-10 IN THE TEN MILE GRABEN AREA
(also Road Log 2)

- Carbonates of Ten Mile Graben and Little Salt Wash Fault
- Curtis and Summerville Formations
- Little Grand Manganese District

Carbonates of Ten Mile Graben and Little Salt Wash Fault

Bill Hood

This paper reviews some of the literature concerning the springs and geysers and the carbonate deposits that are associated with them. It has three sections, the first being a more general review of these features, the second concerning the force of crystallization, and the third reviewing ideas about calcite vs aragonite in the deposits. To make it easier to find a particular reference, they are divided into sections at the end of the paper.

Springs, geysers and carbonate deposits.

The carbonate mineralization, springs and geysers related to faults in the Ten Mile Graben and near Crystal Geyser on the Little Salt Wash Fault have received considerable attention since the first GJGS field trip to this area in 2004. The area has been used to study leaky faults in relation to subsurface carbon dioxide storage (Burnside et al., 2009; Evans et al., 2005; Jung et al., 2014, 2015; Naruk et al., 2019; Shipton et al., 2004; Williams, 2005; and many others). Because the cold spring and geyser deposits were deposited over thousands of years, they have been used to study diagenesis in carbonate rocks (Lima-Zalouomis et al., 2023). Others have used the area to study the eruption of cold-water geysers and their deposits (Barth, 2012; Frery et al., 2017; Gouveia et al., 2004; Gouveia and Friedmann, 2006: Han et al., 2017; Horne et al., 2013; Lagasca, 2022; Lagasca et al., 2021; Watson, 2014). The carbonate deposits have even been used as a partial analogue for features on Mars (Potter-McIntyre, 2013; Potter-McIntyre et al., 2014; Knuth, 2018; Knuth and Potter-McIntyre, 2021; Williams, 2017; Zaloumis, 2021). This list is by no means an exhaustive list, but it should get you started if you want to learn more.

The structural setting of Ten Mile Graben is important in understanding the origin of the springs, geysers and travertine deposits of the area. The Ten Mile Graben cuts across a broad, north plunging anticline whose axis is oriented north-northwestward (heavy red line in **Fig. 1**). Another southward-dipping normal fault, the Little Grand Wash (LGW) fault, cuts the anticline several miles north of Ten Mile Graben. The springs and other features are all located at or very near the northern fault of the Ten Mile Graben and the Little Grand Fault and within about a mile of the anticlinal axis. Many more investigations have centered on the features associated with LGW than those of Ten Mile Graben because it is the location of the active Crystal Geyser, has well-exposed travertine deposits of varying ages and is easily accessible.

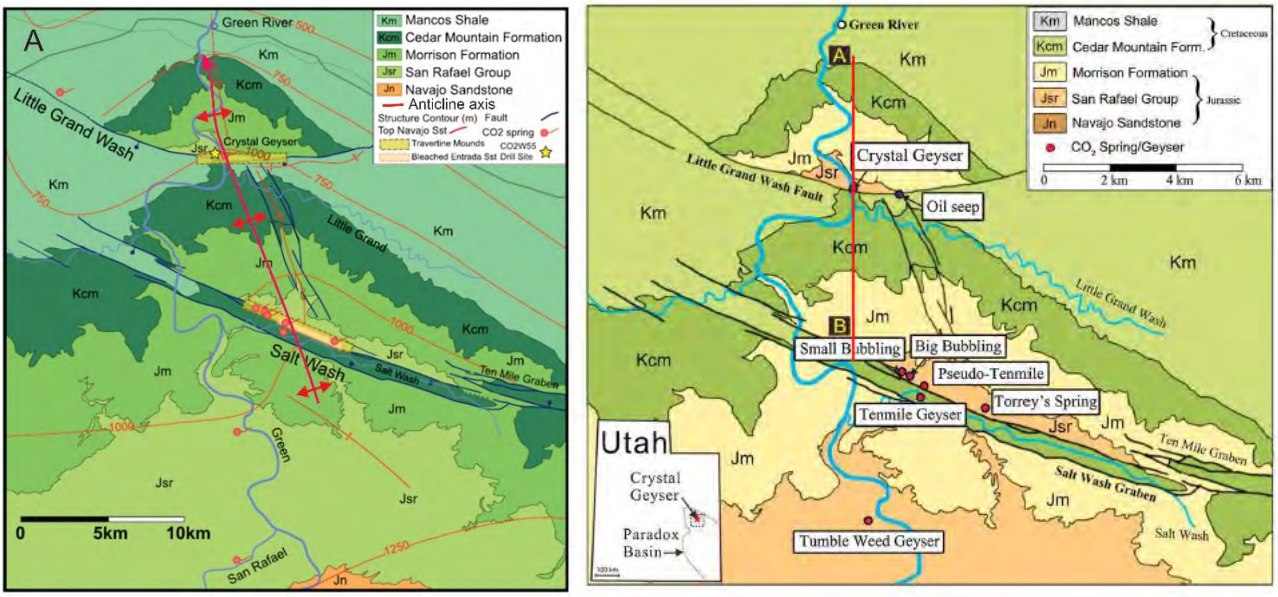

Fig. 1. A. Simplified geologic map of the Ten Mile Graben and Little Grand Wash area. Modified slightly from Kampman et al. (2014b). B. Map showing locations of significant springs and geysers. Source: Jung et al. (2015) fig. 1.

Carbon dioxide gas is actively leaking from the Little Grand Wash fault zone and the Salt Wash (Ten Mile Graben) fault zone. Allis et al. (2005) and Jung et al. (2014) collected soil gas samples and found leakage associated with faults as well as the fault damage area associated with Crystal Geyser. Gouveia et al. (2005) conducted an aerial survey for CO_2 near Crystal Geyser and found as much as119,600 ppm CO_2 in the atmosphere at the time of eruption, compared with less than 400 ppm before and after. Not only is CO_2 leaking, but also water in springs, seeps and geysers. Dating of travertine deposits left behind indicate that some are old, up to 400,000 years old (Burnside et al., 2009; Kampman et al., 2012).

Most studies of the gas have been conducted at Crystal Geyser because it erupts fairly regularly and is easily accessible. Evans et al. (2005) analyzed gas and determined that it was 95 to 97% CO_2. Heath et al. (2009) calculated that the gas was generated at depths > 800 m (> 2625 ft.) and was likely generated by clay-carbonate reactions at temperatures between 100 and 200^o C, although they could not rule out the possible generation by thermal reactions involving igneous intrusions and carbonate rocks. Carbonate rocks (e.g., Leadville Limestone) were deeply buried to depths of over 15,000 feet and attained temperatures greater than 170^o C across large parts of the Paradox Basin (Nuccio and Cobden, 1996) and could have experienced clay-carbonate reactions. Whatever the source, it must have been widespread because CO_2 accumulations appear to be rather common in the Paradox Basin. For example, the Woodside dome, located 19 miles northwest of Green River, UT, is a CO_2-filled structure. Farther away, the McElmo field is a very large CO_2 filled structure containing 97-98% CO_2, and wells in the Lisbon field produce18 to 36% CO_2. Both of these fields are in the Mississippian-age Leadville Limestone (Cappa and Rice, 1995).

Although the CO_2 was likely generated at elevated temperatures, the same was not the case for much of the water involved. The water is cool, not exceeding 18^o C (64^o F). It is saline, ranging from 13,848 to 21,228 ppm TDS (Heath et al., 2009). Hydrogen and oxygen isotope values are consistent with local meteoric water that has not exceeded 500 m in depth. This is consistent with structure and potentiometric surface maps of the Navajo formation in the area (Hood and Patterson, 1984; Naruk et al., 2019). Kampman et al. (2013, 2014b) drilled a well across the Green River from Crystal Geyser and sampled the water contained in the Entrada and Navajo Formations. Watson (2014) sampled water from Crystal Geyser during eruptions. Using his data plus that of Kampman et al. (2014a, 2014b), he calculated that the water in the Crystal Geyser eruptions is about 2/3 Navajo and 1/3 Entrada at the start of an eruption but the relative amounts changed to about 55% and 43% later in the eruption. Deep brines were only 1 to 2 percent of the fluids.

Kampman et al. (2014b) calculated that the brine was saturated with CO_2 at a depth of about 275 m (900 ft). The flash point was estimated to be between 5 to 40 m below the surface. That is consistent with the free gas phase detected by resistivity studies at depths of 5 to 55 m below the surface at Crystal Geyser (Lagasca, 2021). All this leads to the concept of deep subsurface brines charged with CO_2 migrating up faults and into aquifers. If the aquifer is shallower than the flash point, CO_2 gas can exsolve from the brine and leak to the surface, either gradually or in the situation of incompletely cased wells, rapidly in a geyser. This is nicely shown in a figure (**Fig. 2**) by Jung et al. (2015).

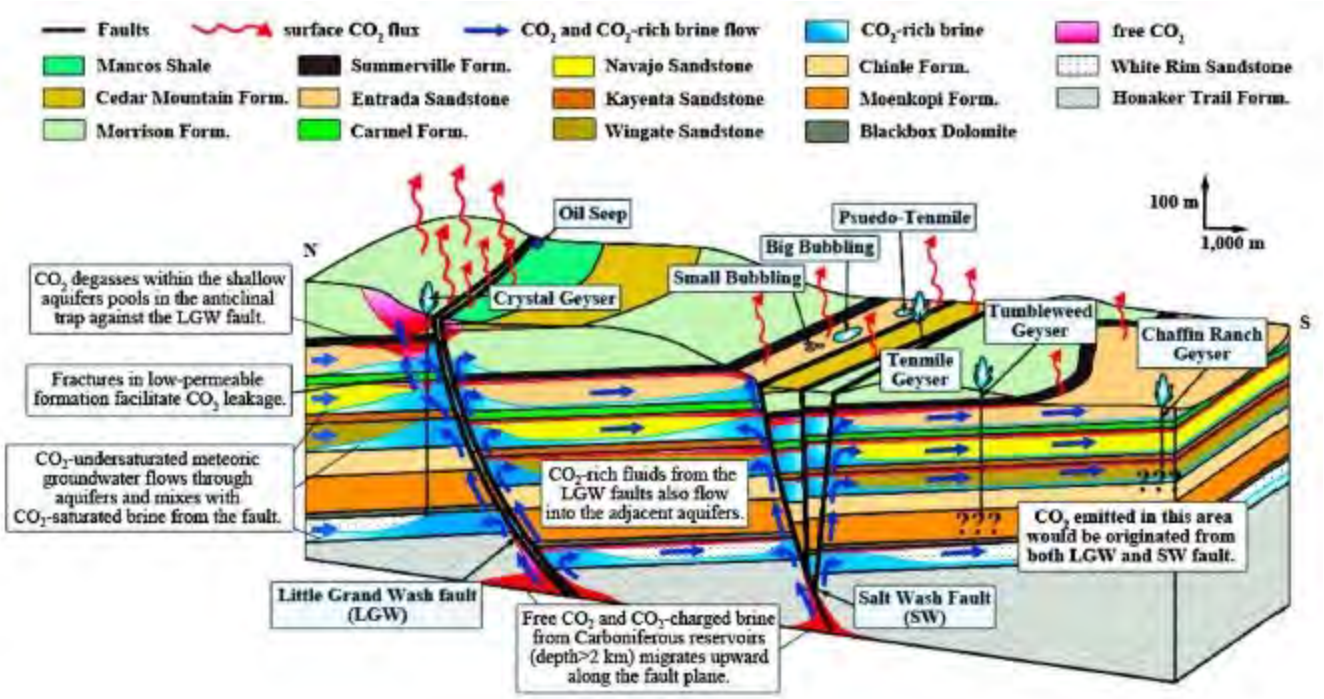

Fig. 2. Block diagram showing conceptual model of migration of CO_2 and brine up Little Grand Wash and Ten Mile graben faults and into aquifers, with leakage along faults and fractures (Jung et al., 2015).

The travertine deposits.

The geochemistry of the carbonate system is fairly simple in concept. It can be explained in a few chemical equations.

1. $CO_2 + H_2O \rightarrow H_2CO_3$ which ionizes to: $H_2CO_3 \rightarrow H^+ + HCO_3^-$

All geologists know that calcium carbonate minerals (calcite and aragonite) dissolve in acid.

2. $H^+ + CaCO_3 \rightarrow Ca^{+2} + HCO_3^-$

Combining these equations:

3. $CO_2 + H_20 + CaCO_3 \rightarrow Ca^{+2} + 2HCO_3^-$

These equations indicate that if the CO_2 is increased, more $CaCO_3$ (calcite) will dissolve. Likewise, if CO_2 is removed from the system, the equations reverse and $CaCO_3$ precipitates.

When any deeply buried rock such as the Leadville Limestone mentioned above contains free CO_2, any water associated with it has to be saturated with CO_2. Fluids in deeply buried rocks are under far greater pressure than a fluid on the surface, either simply due to the weight of the water column, or overpressured because of the weight of the overlying rocks. Under such conditions, much more CO_2 can be dissolved in water than at the surface. (Think about the CO_2 in carbonated drinks). The high pressure drives equation 1 to the right. That, in turn, drives equation 2 to the right, meaning that under pressure, a CO_2-saturated solution will dissolve more calcium carbonate than it can at the surface. If there is sufficient calcium carbonate present, the solution will become saturated under those conditions. When such a solution moves upward into lower pressure, it will become supersaturated with calcium carbonate relative to what it could contain at the surface. This condition will persist as long as there is free CO_2 in contact with the fluid.

When a fluid saturated with CO_2 at great depth and also supersaturated with dissolved $CaCO_3$ approaches the surface, the CO_2 will exsolve into either a supercritical (having characteristics of both a liquid and gas) or a gaseous phase. This will push equation 3 to the right and favor deposition of a calcium carbonate mineral. It is easy to see how this would happen around springs and geysers, where the CO_2 is lost directly into the atmosphere. In the case of carbonate veins, it is not as straight forward. In this case, the CO_2 is lost into porous material, typically a sandstone. Hydraulic overpressure pushes the brine into a fracture in a porous rock. As the fluid moves into the fracture, CO_2 is gradually lost into the surrounding rock. This results in the fluid becoming supersaturated with calcium carbonate, which then begins to be deposited. In some cases, instead of simply filling the fracture and plugging it up, the force of crystallization widens the fracture enough that a film of charged brine can continue to enter the fracture and allow the vein to continue to develop. The escaping water, now depleted of calcium carbonate, has to go somewhere for the vein to continue to develop. It can either continue through the fracture or it, along with the exsolved CO_2, can diffuse into the porous rock. If the system contains some H_2S and the rock contains iron (oxyhydr)oxides, the iron can be reduced and "bleaching" of the rocks occur (Maskell et al., 2018).

The faults of the Ten Mile Graben and the nearby Little Grand Wash fault tap the supercharged and supersaturated water and allow it to move to the near-surface and surface. This reduces the pressure, which allows the CO_2 dissolved in the water to escape. This, in turn, reverses equation 3 and causes the dissolved calcium carbonate to precipitate. This can take the form of carbonate mineral aprons around a spring, seep or geyser, or as carbonate veins in the rock.

Force of Crystallization and Possible Examples in This Area.

We have all seen examples of the force of crystallization whether we have thought about it as such or not. Water freezing is a crystallization process, and we've all seen how it expands in an ice cube tray or how it lifts soil or pebbles when wet ground freezes. You may have also seen sandstone crumble on exposed cliff surfaces where salts are crystallizing in the pore space. Various salts, such as NaCl (halite) and Na_2SO_4 (thenardite) and mirabilite ($Na_2SO_4 \cdot 7H_20$) cause damage to statues monuments, and building exteriors around the world. However, you may not have thought much about its effects on rocks. This section will present a very brief review of some of the voluminous literature on the force of crystallization as it pertains to geology. However, the study of crystallization in confinement is much larger than just geology and if you would like an introduction to the overall literature, the review by Meldrum and O'Shaughnessy (2020) is a good place to start.

One of the early studies that tried to demonstrate the force of crystallization was by Becker and Day (1905). They placed an alum crystal between two glass plates with a load on the upper plate in saturated solution. After a few hours, a detectible uplift of the upper plate and the load was detected. Repeated experiments demonstrated that the growth of the alum crystal could lift a load of up to a kilogram. They also observed that the growth was on the edges of the bottom of the alum crystal, so that as it grew, it created a hollowed-out interior.

A study by Correns and Steinborn (1939) followed. Also using alum, they devised an apparatus to measure the actual growth of a crystal under a given weight. They developed an equation relating the pressure generated by the growing crystal to the degree of supersaturation:

$$P = (RT/V).\ln(K/Ko)$$

Here, T is temperature (degrees Kelvin), R is the ideal gas constant, V is the molar volume of the material under study, K is the product of ionic activity of the solution and K_o is the equilibrium solubility product of the material being studied. In relatively dilute solutions, the concentration, C (g per liter), of the supersaturated solution can be substituted for K and the concentration of the solution at saturation for K_o, giving (C/C_o) as the final term. The equation indicates that the larger the degree of supersaturation, the greater the pressure that the

growing crystal will exert. At saturation ($C = C_o$), there is no net growth and the pressure drops to zero. This equation, or some modification of it, is still used today.

Modern studies have continued to build on those early studies. Desarnaud et al. (2016) studied the pressure generated when halite crystallized from a drop of water between two surfaces. They found that crystal growth could create pressures up to 220 +/- 5 Megapascals, much larger than that needed to break apart grains in a sandstone. They interpreted their results to "suggest that the measured force originates from repulsion between the similarly charged confining wall and the salt crystal separated by a ~1.5 nm liquid film" (p. 1). This method used a fixed amount of starting fluid, and the concentration of salt in the solution would have changed as the solution evaporated, depending on the evaporation rate vs the rate of precipitation.

Li et al. (2017) developed a device that allowed them to observe the growth of a calcite crystal in real time. Their method used a continuous flow of fluid, thus keeping the concentration of ions in the incoming fluid constant. Using an inverted microscope and light interference, they were able to show that growth occurred on the bottom edge of the crystal, leaving a cavity in the interior as it grew. They also established that there was a very thin film of water between the growing crystal and the substrate on which it was growing. In a later paper (Li et al., 2022) they established that with sufficient pressure to reduce the thin film of water to 3 or 4 molecular layers, crystal growth will stop. Gagliardi and Pierre-Louis (2019) developed a numerical model of the growth of a crystal under pressure. Their model indicated that the part of a crystal closest to the source of supersaturation, i.e., the crystal edges, will grow faster, thereby providing a theoretical basis for the observations that growth produces a cavity in the growing crystal.

It should be pointed out that these observations on the force of crystallization require a supersaturated solution that must continually be replenished in order for the crystal or crystals to grow. In nature, there are two ways of doing this, either the fluid migrates along the surface of a crack or it diffuses in from the wall rock. Both possibilities have some difficulties.

Turning to geological observations, one of the early published geologic observations was by Rothrock (1925), who observed calcite veinlets up to 0.2 mm breaking apart quartz grains in a caliche. Minguez and Elorza (1994) used the force of crystallization to in part explain volume for volume replacement.

Van Noort et al. (2017), building on thermodynamic calculations that indicate that the carbonization of peridotite by CO_2 injection, would create enough force of crystallization to create fractures. Their experiments were mostly a failure.

Meng et al. (2018) investigated fibrous calcite veins ("beef veins") in Jurassic-age shale in a basin in the U.K. These veins are usually parallel to bedding and have no indication of faulting or other structural origins. Some of the veins have small openings in the middle, but these do not seem to be connected to anything (**Fig. 3**). They attribute the veins to force of crystallization.

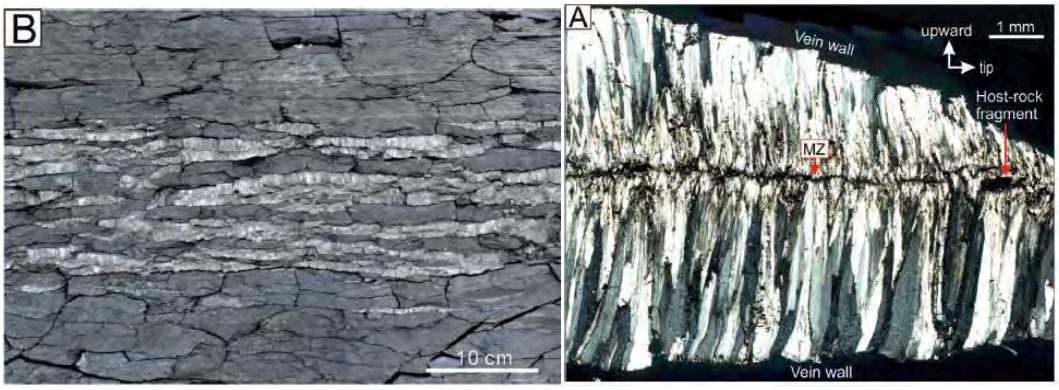

Figure 3. Left, Fig. 2B and right, Fig. 8A from Meng et al. (2018). Left figure shows "beef" veins in shale. Right figure is an enlarged section of a "beef" vein showing the fibrous nature of the calcite and an interior open space.

Wallace and Hood (2018) proposed that the force of crystallization, created by the growth of (typically) dolomite crystals, overcome the tensile strength of rock to product open fractures. These are then filled or partially filled with minerals, creating zebra textures in rocks.

Baraillier (2025) presented an example of gypsum crystals growing in varved clays and deforming the sediment above them. **Figure 4** illustrates this.

Fig. 4. This is Figure 13, p. 13, from Barailler (2025). The sediment above the gypsum crystals has been deformed by crystal growth due to force of crystallization. This occurred with the weight of 20 meters of sediment above it.

The Little Grand Wash fault is located near Green River, Utah, and is similar to the faults of Ten Mile graben. The Crystal Geyser is located along this fault, as are older travertine mounds. Gratier et al. (2012) report on aragonite veins cutting an eroded travertine mound near Crystal Geyser. The veins make up as much as 50% of the mound and are oriented parallel or sub-parallel to the travertine depositional surface. They determined geologic ages on one of these, a 27 cm thick vein. Their results indicate growth of the vein from the top downward, with the top age of 6830 +/- 14 years and the bottom age of 5851 +/- 10 years, or 949 years difference. This showed that the vein grew from the top downward, a process difficult to explain other than by force of crystallization. They also report similar veins extending for tens of meters into nearby sandstones.

At the Ten Mile geyser and travertine quarry stop (#9), we will see examples of veins that are similar to that examined by Gratier et al. (2012) and that can possibly be explained by force of crystallization. For example, in the photo below (**Fig. 5**), how likely is it that a nearly horizontal open space several feet long and perhaps a foot high in a sandstone could have existed long enough for aragonite to fill it? At present the vein is beneath a few feet of overburden, but at the time of deposition, it probably was under more. The force of crystallization lifting the rock as the aragonite "grew" seems a more likely explanation.

Fig. 5. Horizontal carbonate veins (white) in cliff face at the carbonate stop.

Or, consider the contact between the orange and brown areas in the rock pictured below (**Fig. 6**). If the vein were removed, the brown material on the left would drop and match the brown on the right. It is difficult to imagine an open space created like that and persisting long enough to be filled with aragonite. A more probable cause is the force of crystallization pushing the two parts of the rock apart. You undoubtedly will also notice some open space within the vein. Not all parts of the aragonite in the vein need to grow at the same rate. The parts growing faster can continue to push the wall rock apart, creating an open space in other parts of the vein.

Fig 6. Several veins cutting a boulder. The vein mineralogy is probably aragonite, based on

At the Ten Mile geyser and travertine stop (#9), we will examine these features and have a discussion about their origin.

Aragonite or Calcite?

You might wonder why many of these deposits are aragonite rather than the more common form of calcium carbonate, calcite. Aragonite is metastable at the Earth's surface, being stable under high pressures (MacDonald, 1956). That being the case, researchers have wondered why aragonite does not quickly convert to calcite and have attempted to explain it as a result of reaction rates (Fyfe, 1964; Fyfe and Bischoff, 1965).

There is a large amount of literature concerning the question of whether aragonite or calcite will form at the Earth's surface. The information below barely scratches the surface, but it will give you a start if you want to pursue it yourself.

Berner (1975) demonstrated that the presence of Mg ions in concentrations greater than 5% of that of sea water inhibited the growth of calcite. Morse et al. (1997) thought both temperature and Mg/Ca ratios controlled which polymorph of calcium carbonate formed in the modern ocean. Sandburg (1983) recognized oscillations in non-skeletal carbonate mineralogy in marine sediments from aragonite to calcite and back again and attributed it to possible changes in P_{CO2}. Numerous investigators have followed up on that observation. Burton and Walter (1987) concluded temperature was the controlling factor. Others, including Hardy (1996) and Stanley and Hardy (1998), said that aragonite was favored if the Mg/Ca molar ratio was greater than 4. Others (e.g. Ries et al., 2008; Taylor, 2008) considered the switchover occurs at a ratio of 2. On the other hand, Adabi (2004) found aragonite in limestone formed in the shallow part of a basin and mostly calcite in the deeper part and attributed that to temperature, with calcite being favored by colder water. Given and Wilkinson (1985) thought it was the rate of supply of the reactants, particularly the carbonate ion, that governed mineralogy, with high rates of supply of carbonate ions favoring aragonite over calcite and the Mg content having little to do with it.

A totally different idea was presented by Zeng et al. (2018). They did a series of experiments in which they precipitated calcium carbonate in pores of different sizes, and found that the smaller the pore size (i.e., the greater the confinement), the more aragonite was favored.

Examination of active cave features by Gonzalez and Lohmann (1987) let them to conclude that aragonite was favored by high Mg/Ca ratios in cave waters. Both Frisia et al (2002) and Rossi and Lozano (2016) demonstrated that the drip water chemistry influences which calcium carbonate mineral forms, with aragonite being favored over calcite if the molecular ratio of Mg/Ca is greater than about 1.1.

Han et al. (2017) reported the results of water analyses from Crystal Geyser. Their molecular ratios of Mg/Ca (mmol/l) averaged 0.39, well below the ratio that others considered to favor aragonite deposition. Some factor other than Mg must account for the common occurrence of aragonite in this area.

Another element that appears to favor aragonite over calcite is strontium. Sunagawa et al. (2007) examined a travertine deposit in Japan composed of alternating layers of calcite and aragonite. They found that the aragonite layers contained an average of 0.84% Sr whereas the calcite layers contained 0.13%. They also examined several samples of aragonite from other localities and found Sr contents from 0.64 to 4.50%, indicating that Sr can be a common element in aragonite.

We examined 5 samples of travertine from the Ten Mile graben for mineralogy and semi-quantitative chemistry. All of the samples examined were aragonite. The Mg and Sr contents are shown in **Table 1**. Perhaps the presence of Sr in addition to Mg creates the conditions for aragonite to form in this area.

Table 1. Results of XRF analyses of 5 travertine samples from near Ten Mile Geyser.

Sample	Mg %	Sr %
Ten Mile A1	0.46	0.90
Ten Mile A2	0.73	0.95
Ten Mile A3	0.58	0.91
Ten Mile A4	0.53	0.85
Ten Mile dark band	0.53	0.92

Although not directly related to this field trip, but because calcium carbonate is so widely used in industrial applications, a lot of research has gone into methods to control mineralogy, grain size, and grain shape. Declet et al. (2016) and Jimoh et al. (2017) present nice reviews of uses and methods.

References on springs, geysers and carbonates section

Allis, R., Bergfeld, D., Moore, J., McClure, K., Morgan, C., Chidsey, T., Heath, J., and McPherson, B., 2005, Implications of results from CO_2 flux surveys over known CO_2 systems for long-term monitoring: Conference Proceedings, Fourth Annual Conference on Carbon Capture and Sequestration, DOE/NETL, 22 p.

Barth, J. A., 2012, Crystal Geyser, Utah: Active Travertine Deposits of a Cold-water Carbon Dioxide-driven Geyser and Related Ancient Deposits of the Little Grand Wash Fault: M.S. thesis, U. of Houston, 159 p.

Burnside, N. M., Dockrill, B., Shipton, Z. K., and Ellam, R. M., 2009, Dating and constraining leakage rates from a natural analogue for CO_2 storage - The Little Grand Wash and Salt Wash Fault: 2nd International Conference on Fault and Top Seals – From Pore to Basin Scale, CO5, 3 p.

Cappa, J. A. and Rice, D. D., 1995, Carbon dioxide in Mississippian rocks of the Paradox Basin and adjacent areas, Colorado, Utah, New Mexico, and Arizona: U.S. Geological Survey Bulletin 2000-H, 21 p.

Evans, J.P., Heath, J., Shipton, Z.K., Kolesar, P.T., Dockrill, B., Williams, A., Kirchner, D., Lachmar, T.E., and Nelson, S.T., 2005, Natural leaking CO_2-charged systems as analogs for geologic sequestration sites**,** Fourth Annual Conference on Carbon Capture and Sequestration DOE/NETL, www.netl.doe.gov/publications/proceedings/04/carbon-seq/127.pdf

Frery, E., Gratier, J. P. Ellouz-Zimmerman, N., Deschamps, P., Blamart, D., Hamelin, B., and Swennen, R., 2017, Geochemical transect through a travertine mount: A detailed record of CO_2-enriched fluid leakage from Late Pleistocene to present-day – Little Grand Wash fault (Utah, USA): Quaternary International, v. 437, p.98 - 106.

Gouveia, F., Johnson, M. R. Leif, R. N., and Friedmann, S. J., 2005, Aerometric measurement and modeling of the mass of CO_2 emissions from Crystal Geyser, Utah," Lawrence Livermore National Laboratory, Livermore, CA, UCRLTR-212870, 14 p.

Gouveia, F. J. and Friedmann, S. J., 2006, Timing and prediction of CO_2 eruptions from Crystal Geyser, UT: Lawrence Livermore National Laboratory, Livermore, CA,UCRL-TR-221731

Han, W. S., Watson, Z. T., Kampman, N., Grundl, T., Graham, J. P., and Keating, E. H., 2017, Periodic changes in effluent chemistry at cold-water geyser: Crystal geyser in Utah Journal of Hydrology, v. 550, p. 34-64.

Heath, J. E., Lachmar, T. E., Evans, J. P., Kolesar, P. T., and Williams, A. P., 2009, Hydrogeochemical characterization of leaking, carbon dioxide–charged fault zones in east-central Utah, with implications for geologic carbon storage: Carbon Sequestration and Its Role in the Global Carbon Cycle, Geophysical Monograph Series 183, Amer. Geophysical Union, p. 147-158. 10.1029/2006GM000407

Hood, J. W., and Patterson, D. J., 1984, Bedrock aquifers in the northern San Rafael Swell area, Utah, with special emphasis on the Navajo Sandstone: Tech. Publ. No. 78, Utah Department of Natural Resources, Salt Lake City, Utah, 128 p.

Horne, E. A., Evans, J. P., Newell, D., Kampman, N., Nelson, S., and Petrie, E. S., 2013, Field Observations and Geochemical Analysis of Laterally Continuous Aragonite Veins: Insight into Ancient Fluid Travel: Amer. Assoc. Petroleum Geologists Search and Discovery Article #50887.

Jung, N_H., Han, W. S., Watson, Z. T., Graham, J. P., and Kim, K-Y., 2014, Fault- controlled CO_2 leakage from natural reservoirs in the Colorado Plateau, East-Central Utah: Earth and Planetary Science Letters, v. 403. p. 358–367.

Jung, N-H., Han, W. S., Han, K., and Park, E. ,2015, Regional-scale advective, diffusive, and eruptive dynamics of CO_2 and brine leakage through faults and wellbores: J. Geophysics. Res. Solid Earth, v. 120, p. 3003–3025. doi:10.1002/2014JB011722

Kampman, N., Burnside, N., Shipton, Z. *et al.*, 2012, Pulses of carbon dioxide emissions from intracrustal faults following climatic warming: Nature Geoscience, v. 5, p. 352–358. https://doi.org/10.1038/ngeo1451

Kampman, N., Maskell, A., Bickle, M. J., Evans, J. P., Schaller, M., Purser, G., Zhou, Z., Gattacceca, J., Peitre, E. S., Rochelle, C. A., Ballentine, C. J., Busch, A., and Scientists of the GRDP, 2013, Scientific drilling and downhole fluid sampling of a natural CO_2 reservoir, Green River, Utah: Sci. Drill., v.16, p. 33–43. doi:10.5194/sd-16-33-2013

Kampman, N., Bickle, M., Wigley, M., and Dubacq, B., 2014a, Fluid flow and CO_2–fluid–mineral interactions during CO_2-storage in sedimentary basins: Chemical Geology, v. 369, p. 22–50

Kampman, N., Bickle, M. J., Maskell, A. Chapman, H. J., Evans, J. P., Purser, G., Zhou. Z., Schaller, M. F., Gattacceca, J. C., Bertier, P., Chen, F., Turchyna, A. V., Assayag, N., Rochelle, C., Ballentine, C. J., and Busch, A., 2014b, Drilling and sampling a natural CO_2 reservoir: Implications for fluid flow and CO_2-fluid–rock reactions during CO_2 migration through the overburden: Chemical Geology, v. 369, p. 51–82.

Knuth, J. M., 2018, The effects of microorganisms on carbonate precipitation in the Ten Mile Graben cold springs, Utah: A Mars analog: M.S. thesis, Southern Illinois U., Carbondale, IL., 478 p.

Knuth, J. M., and Potter-McIntyre, S. L., 2021, Stable isotope fractionation in a cold spring system, Utah, USA: Insights for sample selection on Mars: Astrobiology, v.21, p. 235-245.

Lagasca, P. A., 2022, Delineating the Shallow Free-phase Gas Distribution at an Abandoned Exploration Well, Crystal Geyser: M.S. thesis, U. of Calgary, 105 p.

Lagasca, P. A., Ryan, M. C., and Bentley, L. R., 2021, Electrical Imaging of a Shallow Free-Phase Stray Gas Plume from an Abandoned Exploration Well: Geofluids, v, 2021, Article ID 2224187, 15 p. 1-15. https://doi.org/10.1155/2021/2224187

Lima-Zaloumis, J., Farmer, J. D., and Trembath-Reichert, E., 2024, Rapid diagenesis and microbial biosignature degradation in spring carbonates from Crystal Geyser, Utah, U.S.A.: Journal of Sedimentary Research, 2024, v. 94, 313–324.

Maskell, A., Scott, P. M., Buisman, I., and Bickle, M., 2018, A siltstone reaction front related to CO_2- and sulfur-bearing fluids: Integrating quantitative elemental mapping with reactive transport modeling: American Mineralogist, v. 103, p. 314–323.

Naruk, S. J., Solum, J. G., Brandenburg, J. P., Origo, P., and Wolf, D. E., 2019, Effective stress constraints on vertical flow in fault zones: Learnings from natural CO_2 reservoirs: AAPG Bulletin, v. 103, p. 1979–2008.

Nuccio, V.F., and Condon, S.M., 1996, Burial and thermal history of the Paradox Basin, Utah and Colorado, and petroleum potential of the Middle Pennsylvanian Paradox Formation: U.S. Geological Survey Bulletin 2000-O, 41 p.

Potter-McIntyre, S. L., 2013, Biogeochemical signatures in iron (oxyhyro)oxide diagenetic precipitates: Chemical, mineralogical and textural markers: PhD Dissertation, University of Utah, 212 p.

Potter-McIntyre, S. L., Chan, M. A., and McPherson, B. J., 2014, Textural and mineralogical characteristics of microbial fossils associated with modern and ancient iron (oxyhydr)oxides: Terrestrial analogue for sediments in Gale Crater: Astrobiology, v. 14, p.1-14.

Shipton, Z.K., Evans, J.P., Kirchner, D., Kolesar, P.T., Williams, A.P., and Heath, J., 2004, Analysis of CO_2 leakage through "low-permeability" faults from natural reservoirs in the Colorado Plateau, southern Utah. *in*: Baines, S. J. & Worden, R. H., (eds.). Geological Storage of Carbon Dioxide, Geological Society, London, Special Publications 233, p. 43-58.

Watson, Z., 2014, An Analysis of CO_2-Driven Cold-Water Geysers in Green River, Utah and Chimayo, New Mexico: M.S. thesis, The University of Wisconsin-Milwaukee, 99 p.

Williams, A. P., 2005, Structural Analysis of CO_2 Leakage Through the Salt Wash and Little Grand Wash Faults from Natural Reservoirs in the Colorado Plateau, Southeastern Utah: M.S. thesis, University of Utah, Logan, Utah, 107 p.

Williams, J., 2017, Sedimentology, mineralogy, and astrobiological implications of spring deposits in Ten Mile Graben, Utah: M.S. thesis, Southern Illinois University, Carbondale, IL, 100 p.

Zaloumis, J., 2021, Investigating biosignature preservation potential of chemical sediments in serpentinites, playa lakes, and spring deposits as potential analogs to planetary environments: PhD dissertation, Arizona State U., Tempe, AZ, 185 p.

Force of Crystallization References

Barailler, B., 2025, The force of crystallization: When gypsum tears the varves of the Trièves!: HAL Id: hal-05169827. https://hal.science/hal-05169827v1

Becker, G. F. and A. L. Day, 1905, The linear force of growing crystals: Proceedings of the Washington Academy of Sciences, v. 7, p. 283-288.

Correns, C. W. and W. Steinborn, 1939, Experimente zur Messung und Erklärung der sogenannten Kristallisationskraft, Zeitschrift für Kristallographie: Crystalline Materials, v. 101, p. 117–133. https://doi.org/10.1524/zkri.1939.101.1.117

Desarnaud, J., Bonn, D., and Shahidzadey, N., 2016, The pressure induced by salt crystallization in confinement: Sci. Rep. *v.* 6, 30856, 8 p. doi:10.1038/srep30856.

Gagliardi, L. and Pierre-Louis, O., 2019, The nonequilibrium crystallization force: arXiv:1909.00414v1, p. 1-7.

Gratier, J. P., Frery, E., Deschamps, P., Røyne, A., Renard, F., Dysthe, D., and Hamelin, B., 2012, How travertine veins grow from top to bottom and lift the rocks above them: The effect of crystallization force: Geology, v. 40, p.1015-1018.

Li, L., Kohler, F., Røyne, A., and Dysthe, D. K., 2017, Growth of calcite in confinement: Crystals, v. 7, article 316, 15 p. doi:10.3390/cryst7120361

Li, L., Kohler, F., Dziadkowiec, J., Røyne, A., Espinosa Marzal, R. M., Bresme, F., Jettestuen, E., and Dysthe, D. K., 2022, Limits to crystallization pressure: Langmuir, v.38, p. 11265−11273.

Meldrum, F. C., and O'Shaughnessy, C., 2020, Crystallization in confinement: Adv. Mater. **2020**, 32, 2001068, 64 p.

Meng, Q., Hooker, J. and Cartwright, J., 2018, Displacive widening of calcite veins in shale: Insights into the force of crystallization: Journal of Sedimentary Research, v. 88, p. 327–343. http://dx.doi.org/10.2110/jsr.2018.18
Menguez, J. M., and Elorza, J., 1994, Diagenetic volume-for-volume replacement: Force of crystallization and depression of dissolution: Mineral. Magazine, v. 58, p. 135-142.
van Noort, R., Wolterbeek, T. K. T., Drury, M. R., Kandianis, M. T., and Spiers, C. J., 2017, The force of crystallization and fracture propagation during in-situ carbonation of peridotite: Minerals 2017, 7, 190, 31p. doi:10.3390/min7100190
Rothrock, E. P., 1925, On the force of crystallization of calcite: Jour. of Geology, v. 33, p. 80-83.
Wallace, M. W., and Hood, A. v.S., 2018, Zebra textures in carbonate rocks: Fractures produced by the force of crystallization during mineral replacement: Sedimentary Geology, v. 368, p. 58–67.

References on aragonite or calcite

Adabi, M., 2004, A re-evaluation of aragonite versus calcite seas: Carbonates and Evaporites, v. 19, no. 2, p. 133-141.
Berner, R.A., 1975. The role of magnesium in the crystal growth of calcite and aragonite from sea water. Geochimica et Cosmochimica Acta, v. 39, p. 489–494.
Burton E. A. and Walter L. M. (1987) Relative precipitation rates of aragonite and Mg calcite from seawater; temperature or carbonate ion control? Geology, v. 15, p. 111–114.
Declet, A., Reyes, E. and Suarez, O. M., 2016, Calcium carbonate precipitation: a review of the carbonate crystallization process and applications in bioinspired composites: Rev. Adv. Mater. Sci., v. 44, p. 87-107.
Frisia, S., Borsato, A., Fairchild, I. J., McDermott, F., and Selmo, E. M., 2002, Aragonite-calcite relationships in speleothems (Grotte de Clamouse, France): Environment, fabrics and carbonate geochemistry: Sedimentary Research, v. 72, p. 687–699.
Fyfe, W. S. (1964). Calcite-aragonite problem. AAPG Bulletin, v. 48, p. 526-526.
Fyfe, W. S. and Bischoff, J. L, 1965, The calcite-aragonite problem: *in* Pray, L. C. and Murray, R. C., (eds.), Dolomitization and Limestone Diagenesis: SEPM Special Publication v. 13. https://doi.org/10.2110/pec.65.07.0003
Given, R. K., and Wilkinson, B. H., 1985, Kinetic control of morphology, composition, and mineralogy of abiotic sedimentary carbonates: Jour. of Sedimentary Petrology, v. 55, p. 109-119.
Gonzalez, L.A., and Lohmann, K.C., 1987, Controls on mineralogy and composition of spelean carbonates: Carlsbad Cavern, New Mexico, *in* James N.P., and Choquette, P.W., (eds.), Paleokarst: New York, Springer-Verlag, p. 81–101.
Han, W.S., Watson, Z.T., Kampman, N., Grundl, T., Graham, J.P., Keating, E., 2017, Periodic changes in effluent chemistry at cold-water geyser: Crystal Geyser in Utah: Journal of Hydrology, v. 550, p. 54-64. doi:http://dx.doi.org/10.1016/j.jhydrol.2017.04.030
Hardie, L.A., 1996. Secular variation in seawater chemistry: an explanation for the coupled secular variation in the mineralogies of marine limestones and potash evaporites over the past 600 m.y.: Geology, v. 24, p. 279–283.
Jimoh, O. A., Ariffin, K. S., Hussin, H. B., and Temitope, A. E., 2017, Synthesis of precipitated calcium carbonate: a review: Carbonates and Evaporites, published online, March, 2017, 16 p. doi 10.1007/s13146-017-0341-x
MacDonald, G. J. F., 1056, Experimental determination of calcite aragonite equilibrium relations at elevated temperatures and pressures: Amer. Mineralogist, v. 41, p. 744-756.
Morse, J.W., Wang, Q., and Tsio, M.Y., 1997, Influences of temperature and Mg/Ca ratio on CaCO3 precipitates from sea water: Geology, v. 25, p. 85-87.
Ries, J. B., Anderson, M. A., and Hill, R. T., 2008, Seawater Mg/Ca controls polymorph mineralogy of microbial $CaCO_3$: A potential proxy for calcite-aragonite seas in Precambrian time: Geobiology, v. 6, p. 106–119.
Rossi, C., and Lozano, R. P., 2016, Hydrochemical controls on aragonite versus calcite precipitation in cave dripwaters: Geochimica et Cosmochimica Acta v. 192, p. 70–96.
Sandberg, P.A., 1983, An oscillating trend in Phanerozoic nonskeletal carbonate mineralogy: Nature, v. 305, p. 19–22,
Stanley, S. M., and Hardie, L. A., 1998, Secular oscillations in the carbonate mineralogy of reef-building and sediment-producing organisms driven by tectonically forced shifts in seawater chemistry: Palaeogeography, Palaeoclimatology, Palaeoecology, v. 144, p. 3–19.
Sunagawa, I., Takahashi, y., and Imai, H., 2007, Strontium and aragonite-calcite precipitation: Jour. of Mineralogical and Petrological Sciences, v. 102, p. 174-181.
Taylor, P. D., 2008, Seawater chemistry, biomineralization and the fossil record of calcareous organisms: *in* Okada, H., Mawatari, S.F., Suzuki, N. and Gautam, P. (eds.), Origin and Evolution of Natural Diversity, Proceedings of International Symposium "The Origin and Evolution of Natural Diversity", 1–5 October 2007, Sapporo, p. 21–29.
Zeng, M., Kim, Y-Y., Anduix-Canto, C., Frontera, C., Laundy, D., Kapur, N., Christenson, H. K., and Meldrum, F. C., 2018, Confinement generates single-crystal aragonite rods at room temperature: *Proceedings of the National Academy of Sciences* (PNAS), v. 115, p. 7670-7675.

Curtis and Summerville Formations

Bill Hood

The Curtis and Summerville Formations comprise an unconformity-bounded pair that record the last intrusion and retreat of the Jurassic inland sea. The lower bound is the J-3 unconformity of Pipiringos and O'Sullivan (1978), with the Curtis lying on the eroded surface of the Entrada Formation. Fossil evidence (Wilcox, 2007; Wilcox and Currie, 2008) indicate that the Curtis Formation is Oxfordian in age. Oxfordian spans the time interval between 161.5 and 154.8 million years old (International Commission on Stratigraphy, 2026). The Curtis Formation grades upward into the Summerville Formation, suggesting that the Summerville is not much younger. The Summerville is bound on the top by the J-5 unconformity, which means that the true depositional thickness in this area is unknown. The overlying unit is the Morrison Formation. Kowallis et al. (1998) analyzed zircons from an ash bed 3 meters above the Morrison – Summerville contact and obtained an age of 155 Ma, which is also Oxfordian. That means that the entire Curtis-Summerville sequence is of Oxfordian age.

The Jurassic Western Interior Seaway, also known as the Sundance Sea, extended into Utah as far south as the Hanksville, Utah, area (Peterson, 1994a, b), the southernmost known occurrence of the Curtis Formation. This is illustrated in **Fig. 1**.

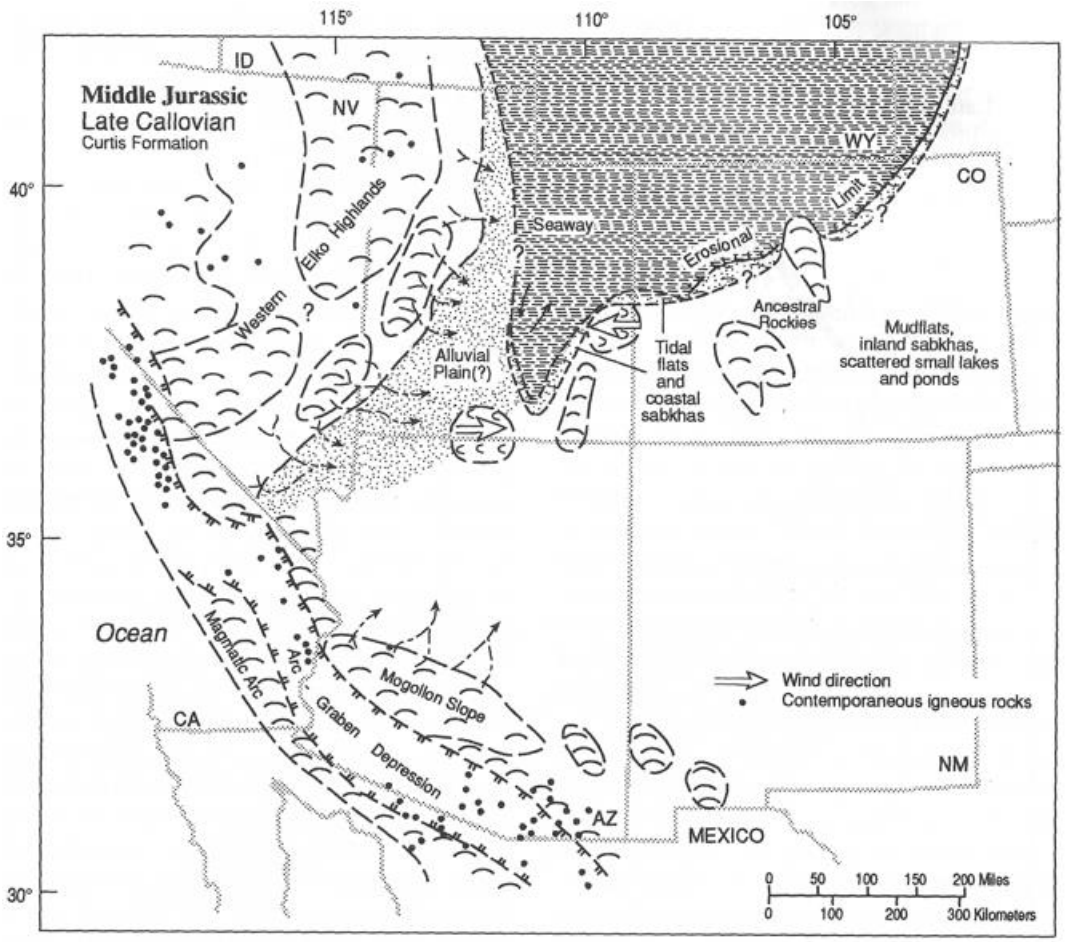

Fig. 1. Paleographic map of the southern part of the Western Interior basis during Curtis Formation time. This is Figure 18 of Peterson (1994).

In Utah, the seaway occupied a foreland basin that was bounded on the west by an elevated plateau that was present in Nevada. To the south, the Mogollon Highlands were shedding sediment northward (Lawton, 1994). The remnants of the late Paleozoic Ancestral Rockies made the eastern border. Western North America had long

been in an arid climate, the wind deposits of the Wingate Sandstone, the Navajo Sandstone and the Entrada Formation attesting to that fact.

Curtis Formation

Overall, the Curtis Formation can be described as a greenish-gray, somewhat glauconitic sandstone 30 to 250 feet thick. The lowermost part begins with conglomerate deposits filling valleys cut into the underlying Entrada Formation (Currie et al., 2005). Above this, the grain size varies from very fine to coarse, and the unit contains both conglomerate and mudstone in places (Wilcox, 2007; Wilcox and Currie, 2008)). Compositionally, the sandstones been described as subarkose and subarenite (Caputo and Pryor, 1991). (In the Folk classification, that means that the rocks contain between 5 and 25% feldspar or rock fragments, respectively). Caputo and Pryor (1991) divide the Curtis into three main facies, a sandstone-mudstone facies, a composite sandstone facies, and a rippled silty facies. The sandstone- mudstone facies is not everywhere present and in places it can contain gravel. Fragments of older units can also be present. The composite sandstone facies is the most extensive and thickest part of the formation. It is the typical greenish-gray, spheroidal weathering sandstone of the Curtis. The rippled silty facies is a fining upward sequence that is transitional into Summerville and is best developed in the southern part of the basin. Wilcox (2007) and Wilcox and Currey (2008) recognized five different facies, and Zuchuat et al. (2018) recognized 24 facies in three subdivisions, not all of which were present in any one outcrop. Kyle et al. (2015) describe zones that contain silicified nodules, some hollowed and celestine-bearing, near the top of the formation on the eastern flank of the San Rafael Swell. They also describe the occurrence of glauconite in thin-sections of the sandstone, but green chlorite as determined by x-ray diffraction in the geodes. This leads to the question of whether the green material called glauconite is really glauconite or chlorite.

Ever since Kreisa and Moiola (1986) recognized internal features of the Curtis Formation as being generated by tides, is has been extensively studied, with the interpretations becoming increasingly more detailed as sedimentologists' understanding of tidal deposits increased (Caputo and Pryor, 1991; Wilcox, 2007; Wilcox and Currey, 2008; Zuchuat et al., 2018, 2019a, 2019b). More recently, Zuchuat et al. (2022) made a mathematical model of the tides of the Sundance Sea. They were able to account for many of the sedimentary features observed in the Curtis Formation and concluded, among other things, that the Curtis arm of the sea was 40 to 45 meters deep in its deepest part. They also have some nice photographs of tidal features preserved in the Curtis. (**Fig. 2**).

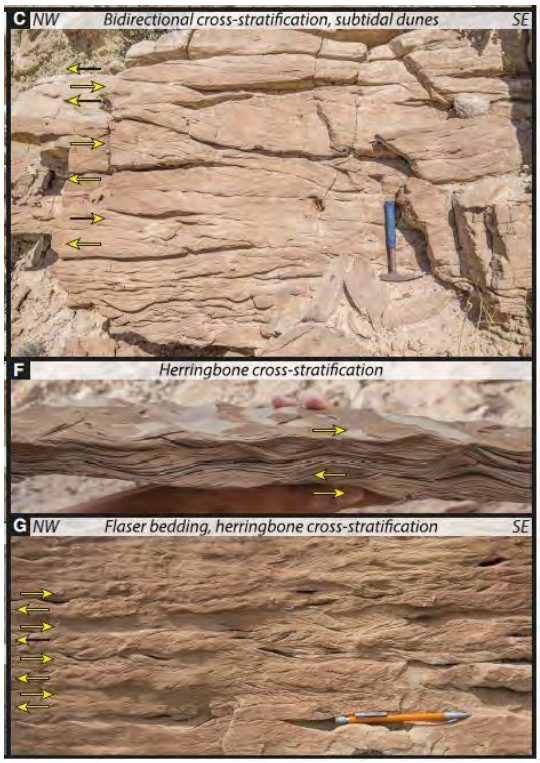

Fig. 2. Some tidal features in the Curtis Formation. This is part of Figure 2 of Zuchuat et al. (2022).

One might wonder about the source for the sand in the Curtis Formation. Prior to the invasion of the Curtis Sea, the area was in the desert belt and the Entrada Formation covered the area. That is not an environment in which significant streams are likely to occur. Some material may have reached to sea from the Mogollon Highlands in southern Arizona. The Ancestral Rockies were either gone or almost gone, because Entrada Sandstone had covered much of the area. Thus, there was probably no large amount of sediment arriving from the east. Some material may have entered from the higher area to the west, but with evidence of a dry climate preserved in the overlying Summerville Formation, that contribution would likely have been small. None of the outcrops that have been studied suggest that they were close to the western shore, so any contributions from that direction would be pure conjecture. Therefore, most of the sand in the Curtis Formation would most likely have been derived from the Entrada Formation.

Summerville Formation

The Summerville Formation was named by Gilluly and Reeside in 1928 for outcrops at Summerville Point, about 20 miles northeast of Green River, Utah. The formation is rather widespread from eastern Utah into northern New Mexico, although there is controversy about nomenclature and whether it the same unit in New Mexico as in Utah (Condon and Huffman, 1988; Anderson and Lucas, 1992; Peterson, 1988; Condon, 1993; Lucas, 2020; Cather, 2020). The Tidwell Member of the Morrison Formation has also been attributed to the Summerville Formation, but Carpenter (2022) presents strong evidence that it is part of the Morrison Formation.

The Summerville Formation has an aerial extent across much of eastern Utah and down into northern Arizona and New Mexico, although it is questionable if the Summerville in those two states is equivalent to the Summerville in Utah (Lucas, 2020; Cather, 2020). It probably extended to about the Utah – Nevada border on the west and is well-exposed on the western side of the San Rafael Swell, where it is over 300 feet thick. On the east, it thins out near the Utah – Colorado border (Caputo and Pryor, 1991), although the unit now called the Wanaka in Colorado National Monument was formerly called the Summerville Formation.

In the area of the field trip, the Summerville is characterized by alternating tabular layers of fine-grained sandstone or siltstone and mudstone, giving it a distinctly banded appearance. It reminds one of a stack of pancakes of a reddish-brown color. It contains some gypsum beds, especially in the area closer to the town of Green River (Caputo and Pryor, 1991). There is a persistent zone near the top of the Summerville that contains chalcedony, sometimes in red botryoidal forms (Stokes and Holmes, 1954). Gilluly and Reeside (1928), as well as Peterson (1994b), mention that the formation has some limestone in some areas but don't indicate where. They also mention that chalcedony concretions are common, as are gypsum beds and nodules, but these not persistent. Both Caputo and Pryor (1991) and Wilcox (2007) measured numerous Summerville sections west of and around the nose of the San Rafael Swell as well as in the Salt Wash graben area but apparently found no limestone. The only significant mention of limestone is in the reports on the El Grand manganese field (Harder, 1910; Pardee, 1921). The limestone beds are important, because these are related to the sedimentary manganese deposits south of the field trip area. Thomas and Krueger (1946) report limestone in the uppermost Curtis near Vernal, UT, but they did not recognize the Summerville Formation. This brings up the possibility that either the rocks that they called uppermost Curtis are actually Summerville of modern usage, or that a limestone-producing environment extended southward into the Ten Mile graben area when the Summerville was deposited.

Fossils are apparently rare in the Summerville Formation, but there is one interesting occurrence. Mickelson et al. (2004) describe a pterosaur tracksite in the Summerville Formation near Ferron, Utah.

Caputo and Pryor (1988) describe two facies in the Summerville Formation, a reddish-brown silty facies and a gypsiferous facies. They describe the former as subarkose and sublitharenite sandstones interbedded with siltstone and mudstone, giving the facies a distinctly banded appearance. The presence of gypsum, shrinkage cracks, raindrop impressions, and similar feature point to subaerial exposure. Their scarce paleocurrent measurements suggest a clock-wise current rotation when viewed from above, with flow to the northeast measured in outcrops on the western side of the San Rafael Swell and toward the south and southeast east of the Swell closer to Moab. They observed channels cut into the sandstones in the western outcrop belt. The channels are 1 to 5

feet deep by 7 to 25 feet wide. The gypsiferous facies also contains abundant small-scale scours and fills, depositional sequences containing both fining -upward and coarsening upward sequences.

Paleogeographic studies indicate that the North American continent was moving northward during Jurassic time. Kocurek and Dott, (1983) presented maps that that showed the northern migration and indicated that at the time of Summerville Formation deposition, the area was approximately 22 degrees north of the Equator. More recent studies by Buzard and Butler (1992) indicate it was closer to 34 degrees, a value in line with that used by Zuchuat et al. (2018) in their calculation of tidal effects. In today's world, most of the large deserts are located near 30 degrees north and south of the equator, the so-called Horse Latitudes. These are areas of high pressure where dry air from the Hadley Cell descends and heats up, creating arid conditions on the Earth's surface. Assuming that the same configuration was present in the Jurassic, the Summerville Formation would have been deposited in an arid. Assuming that there was not a lot of continental movement between Summerville Formation and Curtis Formation, the Curtis Formation would have also been deposited in an arid climate.

References

Anderson, O. J., and Lucas, S. G., 1992, The Middle Jurassic Summerville Formation, northern New Mexico: New Mexico Geology, v. 14, n. 4 pp. 79-92

Bazard, D. R. and R. F. Butler, 1992, Paleomagnetism of the Middle Jurassic Summerville Formation, east central Utah: Journal of Geophysical Research: Solid Earth**,** v.97, p. 4377-4385. https://doi.org/10.1029/91JB03071

Caputo, M. V., and W, A. Pryor, 1991, Middle Jurassic tide- and wave-influenced coastal facies and paleogeography, upper San Rafael group, east-central Utah: *in* Chidsey, T. C., ed., Geology of Central Utah, Utah Geological Association Publication 19, p. 9-27.

Carpenter, K., 2022, The lithostratigraphic Tidwell Member of the Morrison or Summerville Formations (Upper Jurassic)—who, what, where, when? Geology of the Intermountain West, v. 9, p. 49–114.

Cather, Steven M., 2020, Jurassic stratigraphic nomenclature for northwestern New Mexico: *in* Frey, B. A., S. A. Kelley, K. E. Zeigler, V. T. McLemore, F. Goff, and D. S. Ulmer-Scholle, eds., New Mexico Geological Society Special Publication, v. 14, p. 145–151.

Condon, S. M., and A. C. Huffman , Jr., 1988, Revisions in Nomenclature of the Middle Jurassic Wanakah Formation , Northwestern New Mexico and Northeastern Arizona: *in* Condon, S. M., A. C .Huffman, F. Peterson, and W. M. Aubrey, eds., Revisions to stratigraphic nomenclature of Jurassic and Cretaceous rocks of the Colorado Plateau: U..S. Geological Survey Bulletin 1633- A-C, p. 3-12. doi:10.3133/b1633AC

Condon, S. M., 1993, The Middle Jurassic Summerville Formation, northern New Mexico -- a reply to Anderson and Lucas, 1992: New Mexico Geology, v. 15, no.2, pp.33-37.

Currie, B. S., Schwartz, R. K. and Wilcox, W. T., 2005, Sequence stratigraphy of a regional-scale tidal embayment, Upper Jurassic Curtis and Summerville formations, central Utah: Geological Society of America Annual Meeting, Salt Lake City, Paper 50.

Gilluly, J., and J. B. Reeside,1928, Sedimentary rocks of the San Rafael Swell and some adjacent areas of eastern Utah: U. S. Geological Survey Professional Paper 150-D, p. D61-D110.

Harder, E. C., 1910, Manganese deposits of the United States: U.S. Geological Survey Bulletin. 427, 218 p.

International Commission on Stratigraphy.org/chart, 2026. Accessed May 23, 2026.

Kile, D. E., Dayvault, R. D., Hood, W. C., & Hatch, H. S., 2015, Celestine-bearing geodes from Wayne and Emery Counties, southeastern Utah: Genesis and mineralogy: Rocks & Minerals, v. 90, p. 314-337. DOI: 10.1080/00357529.2015.1034489

Kocurek, G., and R. H. Dott, Jr., 1983, Jurassic paleogeography and paleoclimate of the central and southern Rocky Mountain region: in Reynolds, M. W., and E. D. Dolly, eds., Mesozoic Paleogeography of the West-Central United States: Rocky Mountain Paleogeography Symposium 2, Rocky Mountain Section, Society of Economic Paleontologists and Mineralogists, Denver, CO, p.101-116.

Kowallis, B. J., Christiansen, E. H., Deino, A. L., Peterson, F., Turner, C. E., Kunk, M. J., and Obradovich, J. D., 1998, The age of the Morrison Formation: Modern Geology, v. 22, p. 235.

Kreisa, R. D., and Moiola, R. J., 1986, Sigmoidal tidal bundles and other tide-generated sedimentary structures in the Curtis Formation, Utah: Geological Society of America Bulletin, v. 97, p. 381-387.

Lawton, T. F., 1994, Tectonic setting of Mesozoic sedimentary basins, Rocky Mountain region, United States, in Caputo, M.V., Peterson, J.A., and Franczyk, K.J., (eds.), Mesozoic systems of the Rocky Mountain region, USA: Rocky Mountain Section, Society of Economic Paleontologists and Mineralogists, Special Publication, p. 1-25.

Lucas, S. G., 2020, Jurassic stratigraphy of the southeastern Colorado Plateau, west-central New Mexico: 2020 synthesis: *in* Frey, B. A., S. A. Kelley, K. E. Zeigler, V. T. McLemore, F. Goff, and D. S. Ulmer-Scholle, eds., New Mexico Geological Society Special Publication, v. 14, p. 135-144.

Mickelson, D. L., M. G. Lockley, J. Bishop, and J. Kirkland, 2004, A new pterosaur tracksite from the Jurassic Summerville Formation, near Ferron, Utah: Ichnos, v. 11, p.125-142.

Pardee, J. T., 1921, Deposits of manganese ore in Montana, Utah, Oregon, and Washington: U. S. Geological Survey Bulletin 725-C, pp. 179-201.

Peterson, F., 1988, Stratigraphy and nomenclature of Middle and Upper Jurassic rocks, western Colorado Plateau, Utah and Arizona: in Condon, S. M., A. C .Huffman, F. Peterson, and W. M. Aubrey, 1988, Revisions to stratigraphic nomenclature of Jurassic and Cretaceous rocks of the Colorado Plateau: U.S. Geolojgical Survey Bulletin 1633- A-C, p. 13-56. doi:10.3133/b1633AC

Peterson, F., 1994a, Regional paleogeologic and paleogeographic maps of the Mesozoic systems, Rocky Mountain region, US.: in Caputo, M. V., J. A. Peterson and K. J. Franczyk, eds., Mesozoic Systems of the Rocky Mountain Region, USA: Rocky Mountain Section, Society for Sedimentary Geology, Denver, Colorado, P.65-71.

Peterson, F., 1994b, Sand dunes, sabkhas, streams and shallow seas: Jurassic paleogeography in the southern part of the Western Interior Basin: *in* Caputo, M. V., J. A. Peterson and K. J. Franczyk, eds., Mesozoic Systems of the Rocky Mountain Region, USA: Rocky Mountain Section, Society for Sedimentary Geology, Denver, Colorado, p. 233-272.

Pipiringos, G.N., and O'Sullivan, R.B., 1978, Principal unconformities in Triassic and Jurassic rocks, Western Interior United States; a preliminary survey: *in* Unconformities, correlations, and nomenclature of some Triassic and Jurassic rocks, Western Interior United States: U.S. Geological Survey Professional Paper, 1035-A, p. A1-A29.

Stokes, W. L., and C. N. Holmes, 1954, Jurassic rocks of south-central Utah: in Grier, W., ed., Geology of Portions of the High Plateaus and Adjacent Canyon Lands, Central and South -Central Utah: Fifth Annual Field Conference, Intermountain Association of Petroleum Geologists, Salt Lake City, Utah, p. 34-41.

Thomas, H.D., and M. L. Krueger, 1946, Late Paleozoic and early Mesozoic stratigraphy of Uinta Mountains, Utah: American Association of Petroleum Geologists Bulletin, v. 30, p. 1255-1293.

Wilcox, W. T., 2007, Sequence Stratigraphy of the Curtis, Summerville, and Stump Formations, Utah and Northwest Colorado: M.S. thesis, Miami University, Oxford, Ohio, 108 p.

Wilcox, W. T., and B, S. Currie, 2008, Sequence Stratigraphy of the Jurassic Curtis, Summerville, and Stump Formations, Eastern Utah and Northwest Colorado: *in* Longman, M.W., and Morgan, C.D., eds., Hydrocarbon systems and production in the Uinta Basin, Utah: Rocky Mountain Association of Geologists and Utah Geological Association Publication 37, p. 9–41.

Zuchuat, V., A. R.N. Sleveland, D. A. Sprinkel, A. Rimkus, A. Braathen, and I, Midtkandal, 2018, New insights on the impact of tidal currents on a low-gradient, semi-enclosed, epicontinental basin—the Curtis Formation, east-central Utah, USA: Geology of the Intermountain West, v. 5, p. 131–165.

Zuchuat, V., A. R. Sleveland, R. P. Pettigrew, T. J. Dodd, S. M. Clarke, O. Rabbel, and I. Midtkandal, 2019a, Overprinted allocyclic processes by tidal resonance in an epicontinental basin: the Upper Jurassic Curtis Formation, east-central Utah, USA: The Depositional Record, v. 5, p. 272–305.

Zuchuat, V., I. Midtkandal, M. Poyatos-Mor´e, S. Da Costa, H. L. Brooks, K. Halvosrsen, N. Cote, A. Sundal, and A. Braathen, 2019b. Composite and diachronous stratigraphic surfaces in low-gradient, transitional settings: The J-3 ‘‘unconformity’’ and the Curtiss Formation, east-central Utah, U.S.A: Journal of Sedimentary Research, 2019, v. 89, 1075–1095.

Zuchuat, V., E. Steel, R. P. Mulligan, D. S. Collins, J. A. Mattias Green, 2022, Tidal dynamics in palaeo-seas in response to changes in bathymetry, tidal forcing, and bed shear stress: Sedimentology, 69, 1861–1890.

Little Grand Manganese District

Bill Hood

The Little Grand (formerly spelled Little Grande) manganese district is an area 3 miles wide and perhaps 15 miles long, located about 10 miles south of Highway I-70. Beginning a few miles southeast of the town of Green River, it is roughly parallel to I-70 and follows the outcrop of the Summerville Formation, which contains the ore. Most of the productive locations are south of the Ten Mile – Salt Wash graben complex, but a few prospects and small mines are in the Summerville outcrops north of the grabens. The first use of the Little Grand name for the district seems to be by Harder (1910), and was named after a location on the Rio Grande Western Railroad, 8.8 miles west of Crescent Junction, UT (2.1 mi. west of Floy).

The first (and largest) manganese deposit was discovered by E. T. Wolverton while prospecting in 1900. The Colorado Fuel and Iron Company (CF&I) acquired the main deposit, which in 1903 consisted of 643 acres of patented claims and another 1640 acres of unpatented claims. The company established a mining headquarters, called Riverside, a few miles south of the mine on the Green River, the water source, and built a road from the river to the mine and from there to the railroad at Little Grand. The ore was hauled by a steam engine and specially-built wagon (**Fig. 1**). The pair could haul up to 20 tons of ore at a time. The steam engine required a lot of water, about 100 gallons per mile, which necessitated having five 1,000-gallon water tanks between the mine and the railway. The trip took some time, as the average speed was 4 miles per hour. (Anonymous,1903).

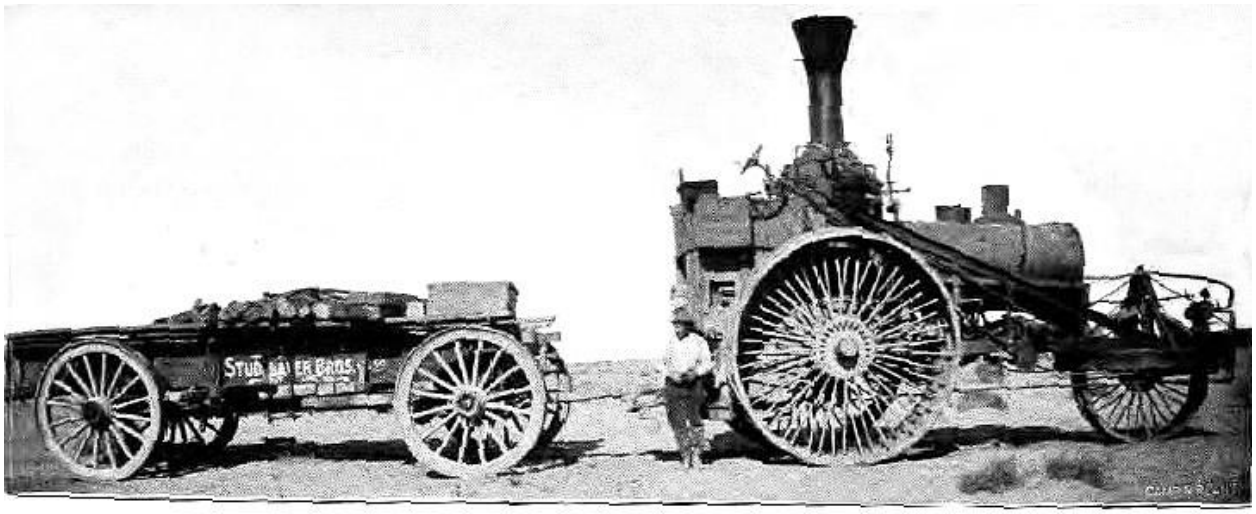

Traction Engine and One of the Wagons Used for Hauling Ore From the Deposits to the Railway.

Fig. 1. The engine and ore wagon in operation by CF&I from 1901 to 1906 (Anonymous, 1903).

The CF&I mine operated in 1901, 1903, 1904 and 1906, producing about 4,000 tons of high-grade ore. Mining ceased until 1915, when prices for manganese increased and made mining potentially profitable again. At that time, three companies operated in the district, producing about 8,000 tons of ore until prices dropped at the end of WWI (Pardee, 1921). No mining occurred up to 1939, when some evaluation work was done in that year and in 1940 (Baker, et al., 1952). I found no more recent information on production although Dick Dayvault (personal communication, 2004) indicated that there was some minor production during the Korean war. The deposits are tiny by today's mining standards.

An early description of the ore bodies was by the reporter for Camp and Plant Anonymous (1903), who reported that the ore followed bedding planes between layers of "Triassic sandstone." He reported that the ore was in multiple layers in well-defined, north-trending channels, with the mineralized zone having a total thickness of about 5 feet. The first geological description of the area is by Harder (1910), who described the deposits as surface blankets, consisting partly of surface float and partly of replacement of red limestones. He described the deposits as occurring at the top of the thin-bedded limestone and sandstone formations and implied that they were possibly an ancient lag accumulation that was later buried and recently exhumed.

Pardee (1921) described the deposits in more detail, pointing out their common association with red limestone. The limestone is in layers up to a foot thick, with layers separated by reddish-brown sandy clay. The limestone interval is 5 to 15 feet thick, with some of the layers locally replaced entirely or partly by manganese mineralization. He described the in-situ deposits as typically thin layers, usually 3 to 5 inches thick, but rarely up to a few feet thick. The individual mineralized zones are typically only a few 10s of feet wide and. where exposed near a cliff edge, do not appear to extend very far back from the edge. The manganese minerals are manganite and pyrolusite. Calcite, gypsum and barite also occur in the ore, and celestine occurs below the ore bodies in places. Pardee also noted that the limestone contains specks of a reddish mineral, possibly rhodochrosite or kutnohorite, that when heated turns black.

Baker et al. (1952) reported that the blanket deposits are all associated with limestone, which is a minor component of the Summerville Formation in the Little Grand district. The manganese mineralization is either in the limestone beds or immediately beneath them. The limestone layers are lenticular and are more extensive than the manganese mineralization. At some locations, there is only one mineralized layer; at others there are several. Most of the lenses are only a few inches thick and small; the largest is only a few hundred feet in maximum dimension. At some locations, there are small veinlets, usually less than 0.5-inch wide. At other places there are sandstones impregnated with manganese minerals, but these are too low grade to be ore. Many of this type of deposit contain a sooty pyrolusite that is not recoverable by the mining methods in use at the deposits.

Two other publications mention the Little Grand district. McKnight (1940) wrote a paragraph about the area in U.S.G.S. Bulletin 908 and Bowman (1960) wrote a short summary of the area, mainly taken from Baker et al., (1952).

Speculation as to the origin.

Pardee (1921, recognized that there were specks of manganese carbonate in the limestones. That prompted him to propose a hypothesis for formation of the ore bodies. He suggested that weathering of the manganese-bearing limestone far up dip from the present ore bodies released manganese into solution. The dissolved manganese migrated in ground water to its present location, where it partially replaced the limestone and filled minor cracks in the underlying sandstone, creating the ore bodies.

There are some problems with Pardee's hypothesis. First is a volume problem. Baker et al. (1952) reported two analyses of Mn in the limestone, 0.02 and 0.48%. They did not indicate whether the values were for Mn or MnO. Assuming the value was for Mn, using the average of those values and the weight of a cubic foot of typical limestone (165 lb.), it would take about 4,850 cubic feet of limestone to produce a ton of Mn. If the analysis value was MnO, the amount of limestone would be 1.3 times higher. To concentrate the 4,000 tons of ore produced at the mine would require 19.4 million cubic feet of limestone to dissolve and the manganese be transported to the mine area. That is a lot of limestone. The second problem is moving the dissolved manganese. Thin beds of

limestone would not be a good aquifer. Could the Mn have been transported to the mine location from somewhere up dip through such an aquifer? The third problem is geochemical. Manganese in the +2-valance state is soluble and easily transported, but the ore has Mn in the +4-valence state. The Mn would have to be mobilized in a somewhat reducing environment and then reprecipitated in an oxidizing environment underground. The combination of these three factors makes Pardee's hypothesis unlikely.

Baker et al. (1954) also pointed out that there appears to be no association with structure and suggest that the manganese may have been deposited with the associated sediments. There are a very large number of sedimentary manganese deposits around the world (Hewett, 1966; Kuleshov, 2010), and they are mostly confined to specific times in Earth history (Kuleshov, 2010; Roy, 2006; Maynard, 2010). These episodes are associated with anoxic events in the ocean (Roy, 2006; Force and Cannon, 1988; Force and Maynard, 1991; Calvert and Pederson, 1996; Xu et al., 2025), which allows manganese to accumulate as Mn+2 in sea water, and with highstands of the sea, which allow the Mn-bearing water to flood onto the continent. There is a growing body of evidence that the Late Jurassic, including the Oxfordian (the age of the Summerville Formation) was a time of low oxygen levels (hypoxia, and perhaps even anoxia in the ocean (Rogov et al., 2020; Gernon et al., 2024). The Summerville Formation represents the retreat from a high stand of the ocean, being the last landward intrusion of the Jurassic Inland Sea into western North America. Such a high stand could have brought Mn-rich water into a shallow, well-oxygenated area during Summerville time, where the manganese would have been oxidized and precipitated as either pyrolusite or manganite. Wilcox (2007) demonstrated that the Summerville is the approximate equivalent to the Redwater Member of the Stump Formation, which occurs near the Uinta Mountains. Within the Redwater Member there is a 15-meter thickness of laminated black shale (Wilcox, 2007). This represents a low-oxygen environment in which any manganese present could have been reduced to the +2-valence state and thus be available for transport by currents. (See Eh-pH diagram below). Dong et Microbes may play a role in sedimentary manganese deposits (Yu et al., 2021; Xu et al., 2024; al., 2024), although this has not been investigated for the Little Grand deposits.

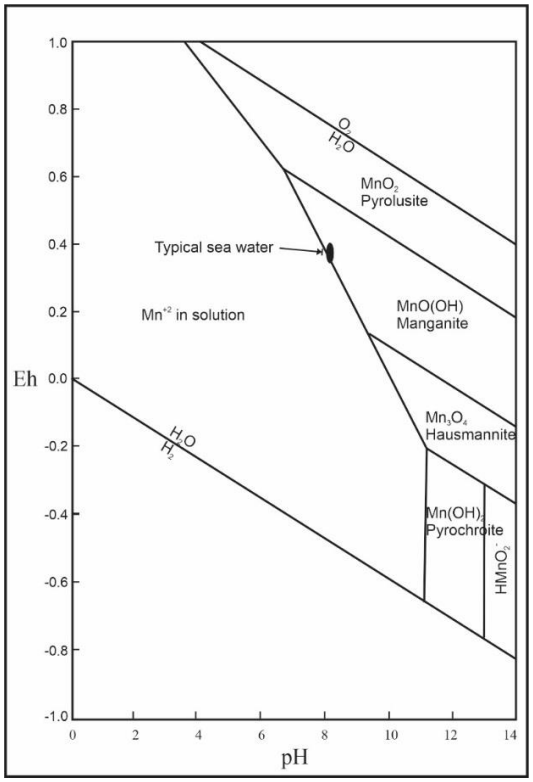

Fig. 2. Eh-pH diagram for manganese showing the position of typical sea water.

Under typical conditions, Mn is nearly insoluble in sea water (**Fig. 2**). However, under anoxic conditions (lower Eh) it is soluble and can accumulate in the water. If such water it transferred by currents into an oxygen-rich environment, it will precipitate as either pyrolusite or manganite. For example:

$Mn^{+2} + H_2O + ½\ O_2 \rightarrow MnO_2 + 2H^+$.

Notice that anything that would use up the hydronium ion will drive the equation to the right and precipitate pyrolusite. If there is calcite around, this can happen:

$2\ H^+ + CaCO_3 \rightarrow Ca^{+2} + H_2CO_2 \rightarrow Ca^{+2} + H_2O + CO_2$.

Oxidation of the Mn^{+2} generates the H^+ ion needed to dissolve the calcite. This gives a nice chemical way to replace limestone with a manganese oxide mineral. We examined 10 randomly collected pieces of manganese ore in the CMU X-ray lab. All of the samples were pyrolusite and all contained a little quartz. Caliche coatings were present on most pieces.

Photographs of manganese ore. Scale is in centimeters.

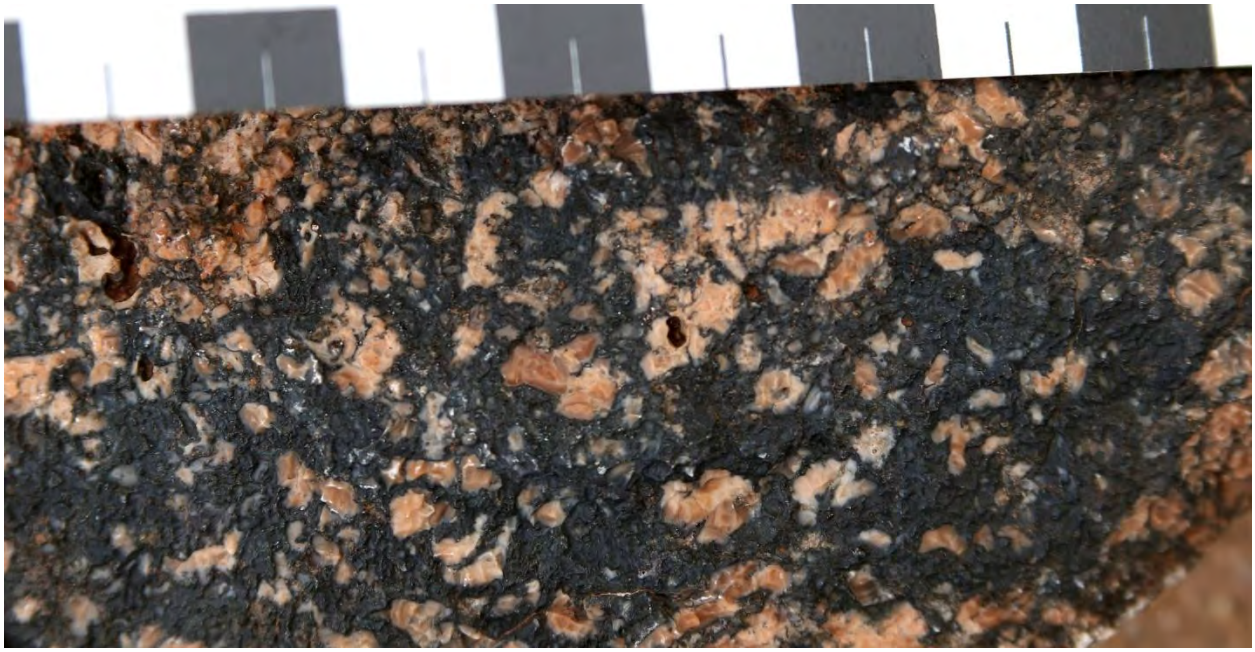

Photo 1. Close-up of manganese mineral with calcite. This may be a piece of replaced lime-stone but it was an isolated piece of float downhill from the old mine so the origin is uncertain.

The photos below are of pieces of manganese ore collected from the old mine area.

Photo 2. Larger pieces of manganese ore. These were found downslope from the old mine.

Photo 3. Small pieces of manganese ore, partly coated with caliche. Pieces like this are abundant scattered on the surface near the old mine.

Photo 4. Caliche coating on a piece of manganese ore. The coating, present on only one side, is up to a half -centimeter thick.

References

Anonymous, 1903, The Little Grande Manganese Mine: Camp and Plant, v. 3, p. 437-439. Published by Colorado Fuel and Iron, Denver and Pueblo, Colorado. https://steelworks.us/wp-content/uploads/2015/08/CP_1903_05_16_V3N19.pdf

Baker, A. A., D. C. Duncan, and C. B. Hunt, 1952, Manganese deposits of southeastern Utah: U.S. Geol. Survey Bull. 979-B, 103 p.

Bowman, F. O., 1960. Manganese deposits of the Little Grand District in southeastern Utah: Geology of the Paradox Basin Fold and Fault Belt, Four Corners Geological Society Third Field Conference, p. 118-119.

Calvert, S. E., and T. F. Pedersen, 1996, Sedimentary geochemistry of manganese: Implications for the environment of formation of manganiferous black shales: Economic Geology, Vol. 91, 1996, pp. 36-47

Dong, Z-G., B-L. Zhang, I. Gyollai, K. Fintor, M. Szabo, I. Kovacs, J. Gao, L-C. Zhang, M. Polgari, and C-L Wang, 2024, Microbial contribution to the formation of the Carboniferous sedimentary manganese deposits in northwestern China: Ore Geology Reviews, v. 170, 106124

Force, E. R., and Cannon, W. F., 1988, Depositional model for shallow-marine manganese deposits around black-shale basins: Economic Geology, v. 83, pp. 93-117.

Force. E. R., and J. B. Maynard, 1991, Manganese: Syngenetic deposits on the margins of anoxic basins: in Force, E.R., Eidel, J.J., and Maynard, J.B., eds., Sedimentary and Diagenetic Mineral Deposits, a Basin Analysis Approach to Exploration: Reviews in Economic Geology v. 5, Society of Economic Geologists, Ch. 11, p.147-157.

Gernon, T. M., *et al*., 2024, Solid Earth forcing of Mesozoic oceanic anoxic events: *Nat. Geosci*, published online August 29, 2024; doi: 10.1038/s41561-024-01496-0

Harder, E. C., 1910, Manganese deposits of the United States: U.S. Geol. Survey Bull. 427, 218 p.

Hewett, D. F.,1966, Stratified deposits of the oxides and carbonates of manganese: Econ. Geol., v. 61, p. 431-461.

Kuleshov, V. N**.,** 2011, Manganese Deposits: Communication 2. Major Epochs and Phases of Manganese Accumulation in the Earth's History: Lithology and Mineral Resources, v. 46, pp. 546–565.

Maynard, J. B., 2010, The chemistry of manganese ores through time: A signal of increasing diversity of Earth-surface environments: Economic Geology, v. 105, pp. 535–552

McKnight, E. T., 1940, Geology of the area between the Green and Colorado Rivers, Grand and San Juan Counties, Utah: U. S. Geol. Survey Bull. 908, 147 p.

Pardee, J. T., 1921, Deposits of manganese ore in Montana, Utah, Oregon, and Washington: U. S. Geol. Survey Bull 725-C, pp. 179-201.

Rogov, M., E. Shchepetova, and V. Zakharov, 2020, Late Jurassic – earliest Cretaceous prolonged shelf dysoxic–anoxic event and its possible causes: Geological Magazine, v. 157, p. 1622-1642. doi:10.1017/S001675682000076X

Roy, S., 2006, Sedimentary manganese metallogenesis in response to the evolution of the Earth system: Earth-Science Reviews, v. 77, p. 273–305.

Wilcox, W. T., 2007, Sequence Stratigraphy of the Curtis, Summerville, and Stump Formations, Utah and Northwest Colorado: M.S. thesis, Miami University, Oxford, Ohio, 108 p.

Xu, H., J. Gao, R. Yang, F. Chen, J. Xu, L. Wang, C. Yang, and R. Yin, 2025, Sedimentary manganese carbonate deposits as faithful proxies of ancient ocean redox fluctuations: Insights from the Permian Zunyi Mn deposits, South China: GSA Bull., v. 137, p. 5148-5162.

Yu, W., M. Polgari, I. Gyollai, K. Fintor, H. Huang, M. Szabo, and Y. Du, 2021, Microbial metallogenesis of early carboniferous manganese deposit in central Guangxi, South China: Ore Geology Reviews, v. 136, p. 1-18.